

Moho Topography and Velocity/Density Model for the Hedmarken area, Eastern Norway, using Receiver Function Analysis and Rj-McMC

Claudia Pavez, Marco Brönnner, Arne Bjørlykke, Odleiv Olesen
Geological Survey of Norway



To follow this presentation

This slide explains how to understand the presentation through the methodological sequence. In the upper right corner of each slide you will find the number that is corresponding to the specific methodologies listed below

VISUALIZATION & GEOGRAPHIC INFORMATION SYSTEMS

0. GMT
QGIS



METHODOLOGY

Seismic processing:

1. IRIS Wilber3
2. SAC

Transdimensional inversion

3. Rj-rf
4. Rj-McMC
(Reversible jump receiver
function & Reversible jum
Markov chain Monte Carlo)

Study area: Central-Eastern Norway, Hedmarken

Table 1: NORSAR large aperture seismic array

Station code	Latitude [°]	Longitude [°]	Elevation [m]
NAO01	60.844	10.886	426
NBO00	61.030	10.777	529
NC204	61.275	10.762	851
NC602	60.735	11.541	305
NB201	61.049	11.293	613
NC405	61.112	11.715	496
NC303	61.225	11.369	401

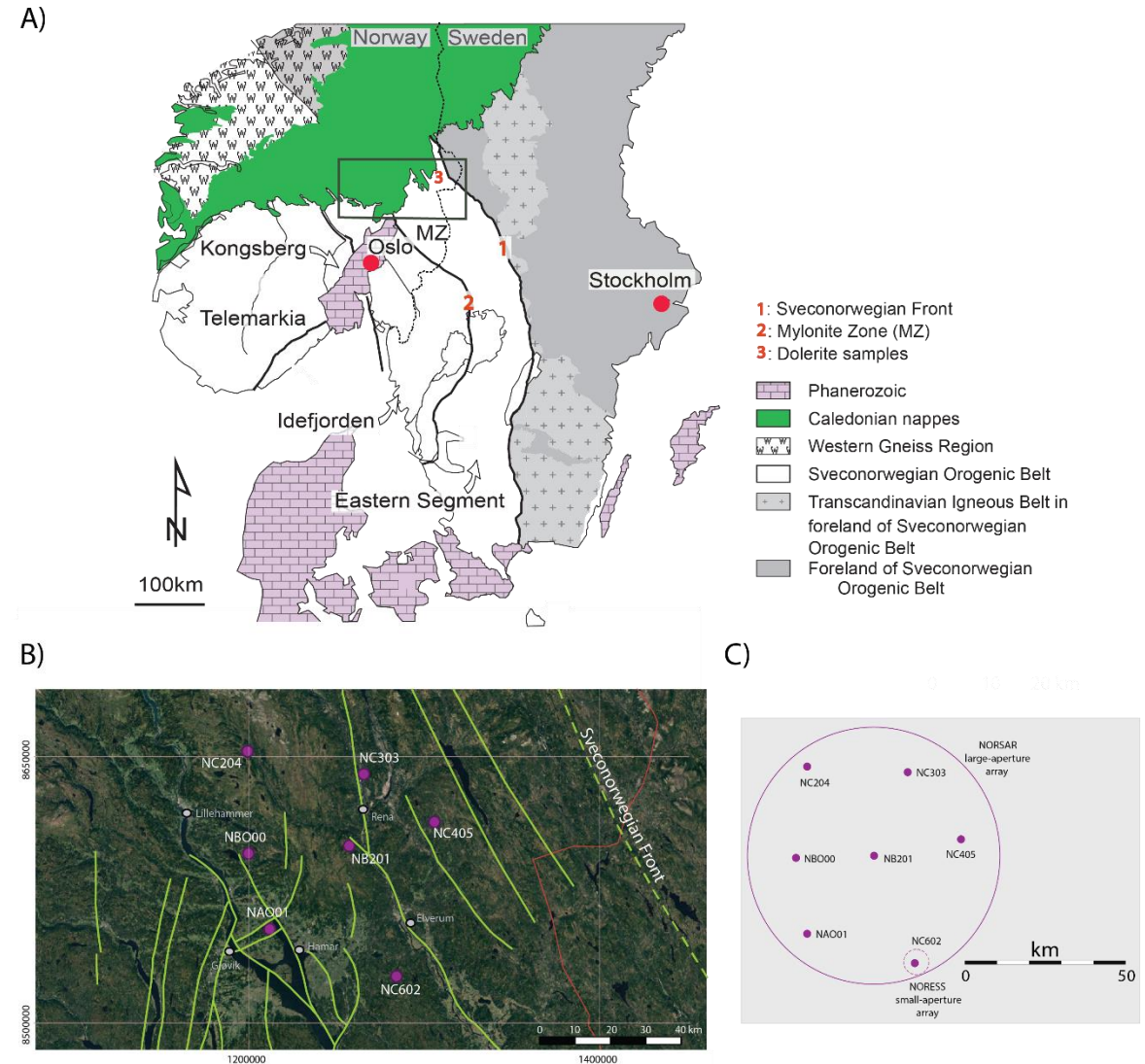
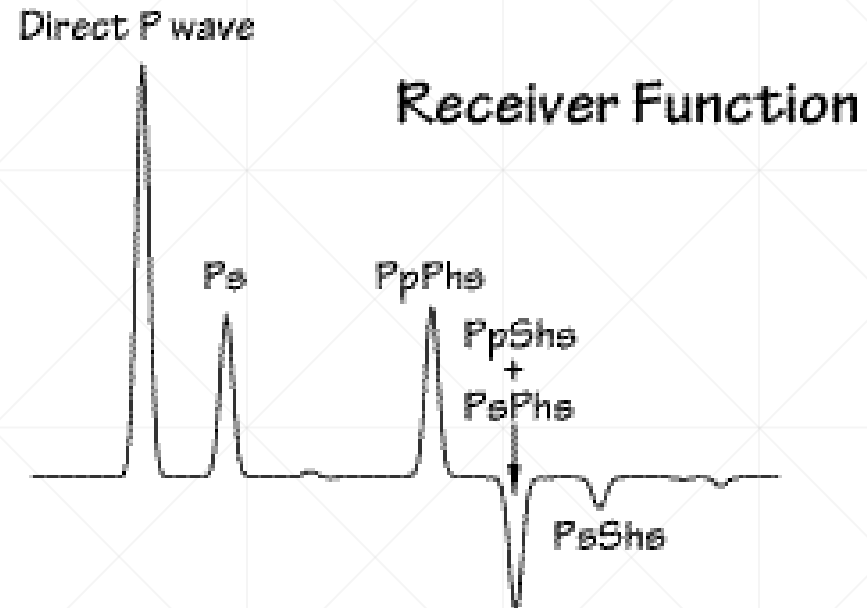


Figure 1: A). Sketch map showing the lithotectonic units of the Sveconorwegian Orogenic Belt (Modified from Bingen & Viola, 2018). The black box is showing the location of the NORSAR array and the interpolation area used in this research B). Digital elevation model showing a zoom-in of the seismic stations. Green lines correspond to the major faults observed in the zone, mainly composed by NS and NNW lineaments near to the array. Dotted green line delineates the Sveconorwegian front. C).

Pavez et al., 2020.

Part I: HK Stacking



*Figure from C. Ammon's receiver function webpage
(see references)*

Recorded teleseismicity

- We used 50 teleseismic events recorded during the 2017-2018 period by the NORSAR array.
- A set of 20 high magnitude events ($M_w \geq 6.0$, $M_b \geq 5.6$) with epicentral distances between $30^\circ - 90^\circ$ was selected according quality.
- The ray parameter (p) was calculated per each event.

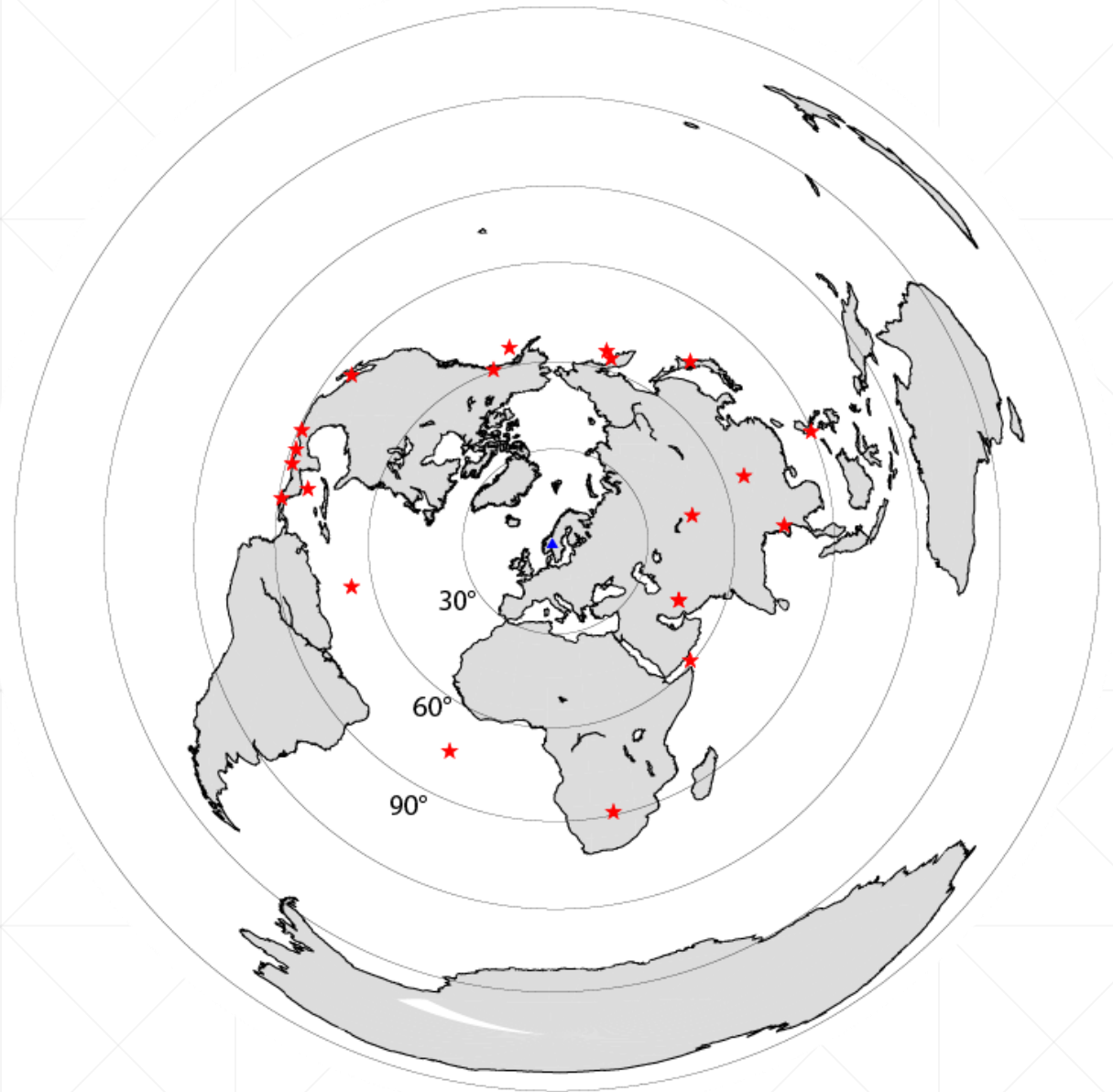
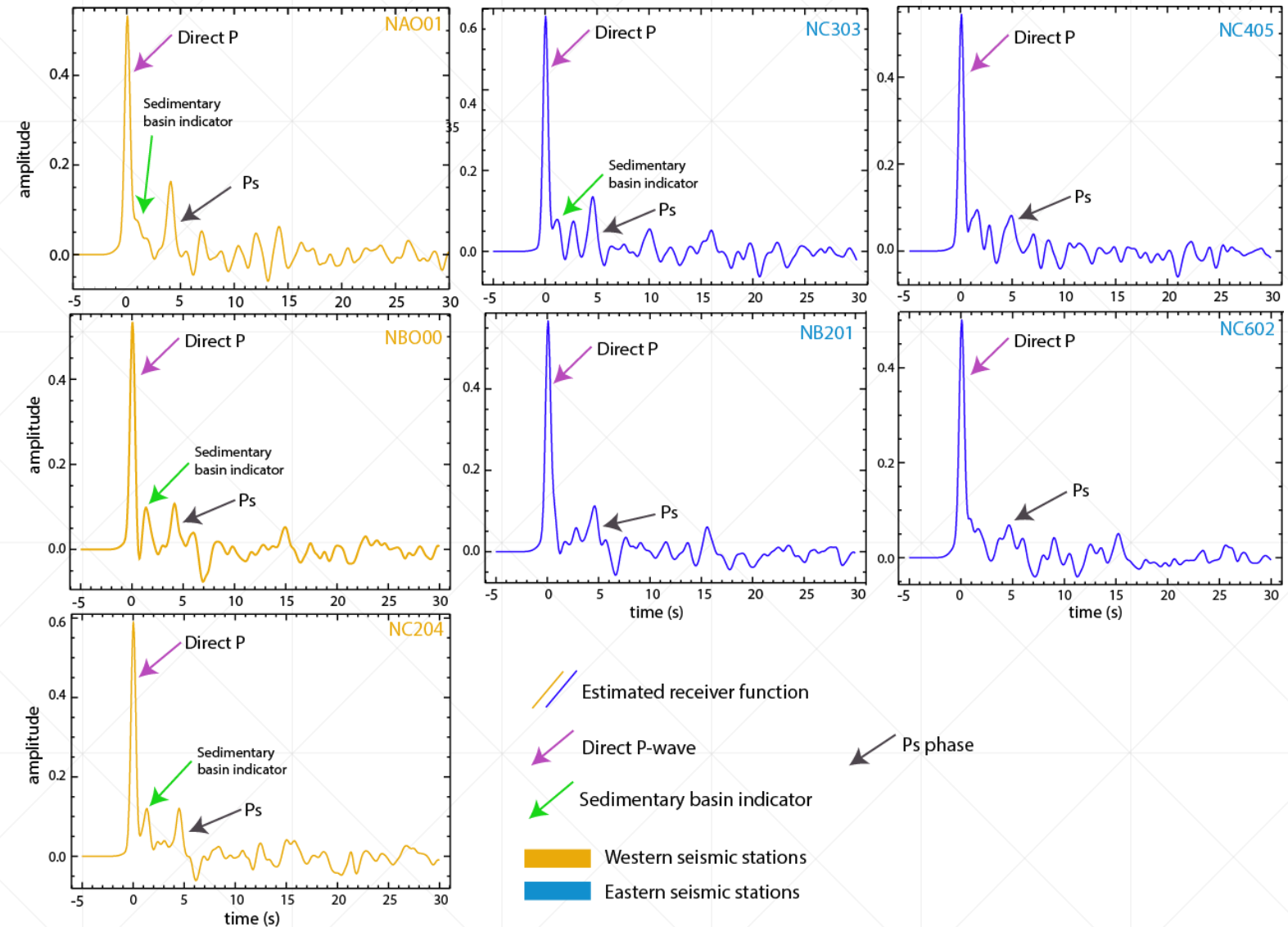


Figure 2: Location of teleseismic events accepted for processing and stacking (red stars). All the events are located between $30^\circ - 90^\circ$ from the study area, centered at NB201 seismic station (blue triangle) (from Pavez et al., 2020)

Receiver functions

The receiver functions were calculated through time-domain deconvolution, using the CPS seismology package (Ligorria & Ammon, 1999; Hermann, 2013)

Figure 3: Stacked & non-scaled receiver functions for each seismic station. The main phases are shown and the intra-crustal discontinuities related to the Åsta basin are marked with a green arrow.



HK Stacking results

According to the receiver functions and the arrival times of the different phases (P and Ps), the HK stacking method was applied.

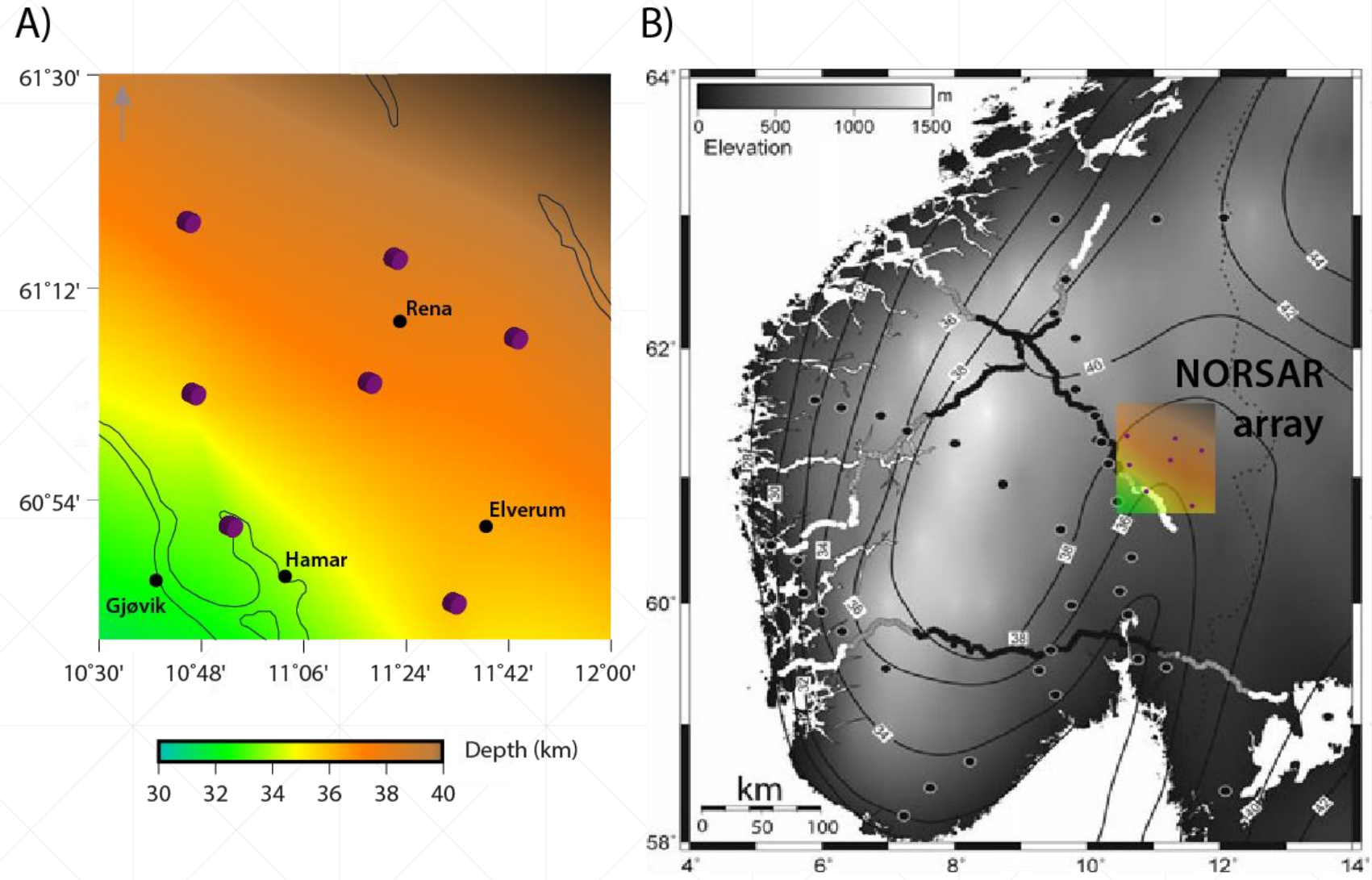
Station	H (km) \pm	K \pm	Poisson's ratio
NAO01	33.5 \pm 0.31	1.72 \pm 0.015	0.245
NBO00	35.3 \pm 0.30	1.71 \pm 0.02	0.240
NC204	37.8 \pm 0.31	1.76 \pm 0.015	0.262
NC602	35.9 \pm 0.40	1.78 \pm 0.05	0.269
NB201	37.1 \pm 0.31	1.73 \pm 0.01	0.249
NC405	37.8 \pm 0.67	1.79 \pm 0.09	0.273
NC303	38.4 \pm 0.31	1.71 \pm 0.02	0.240

Table 2: HK Stacking results per station, including projected errors. The western cluster is shown in orange and the eastern one in blue.

Mohorovicic depth: 2D projection

Figure 4: A. Local crustal thickness beneath the NORSAR network. Purple circles correspond to the location of seismic stations.

B. Original Moho map for Southern Norway proposed by Stratford et al., (2009). The original image was modified overlapping the results obtained in this research for comparative purposes.



Part II: Transdimensional inversion

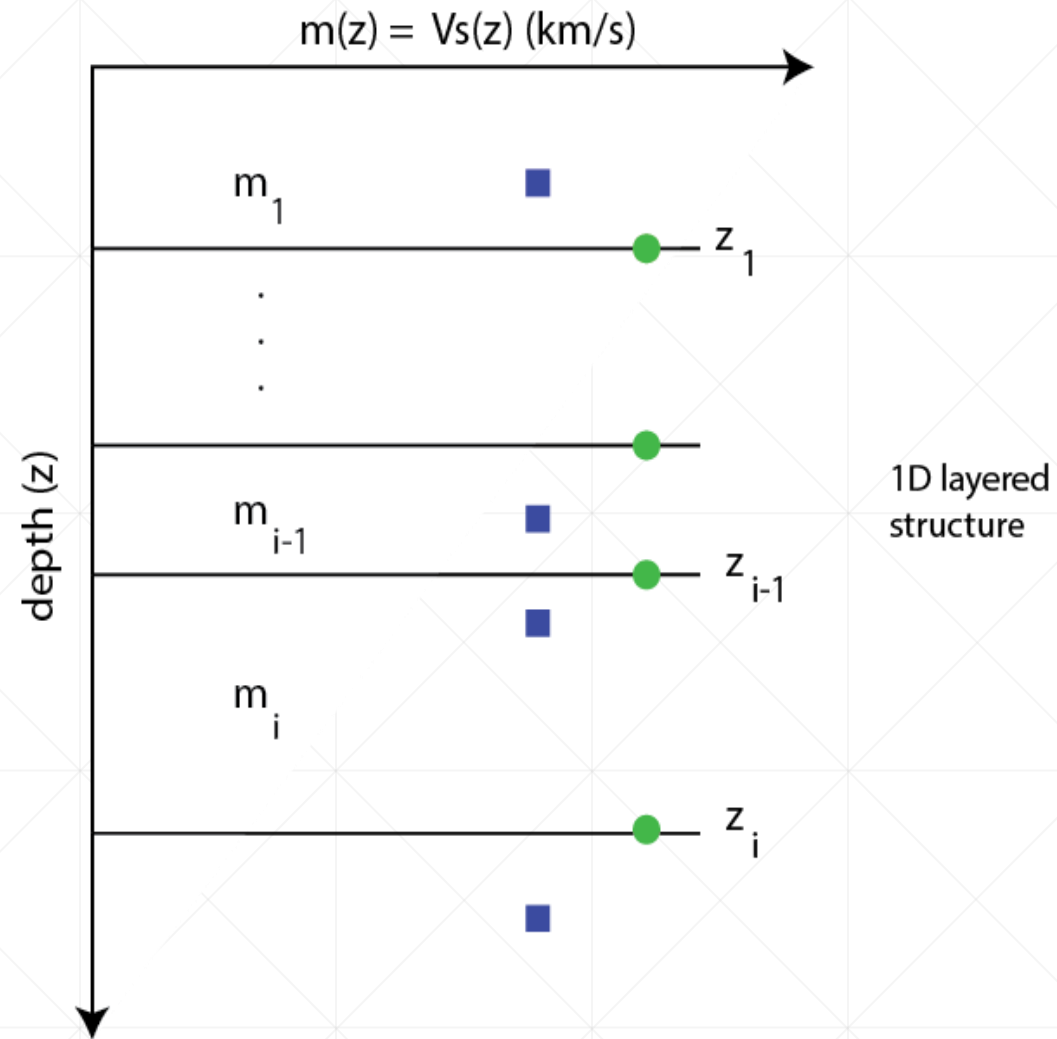


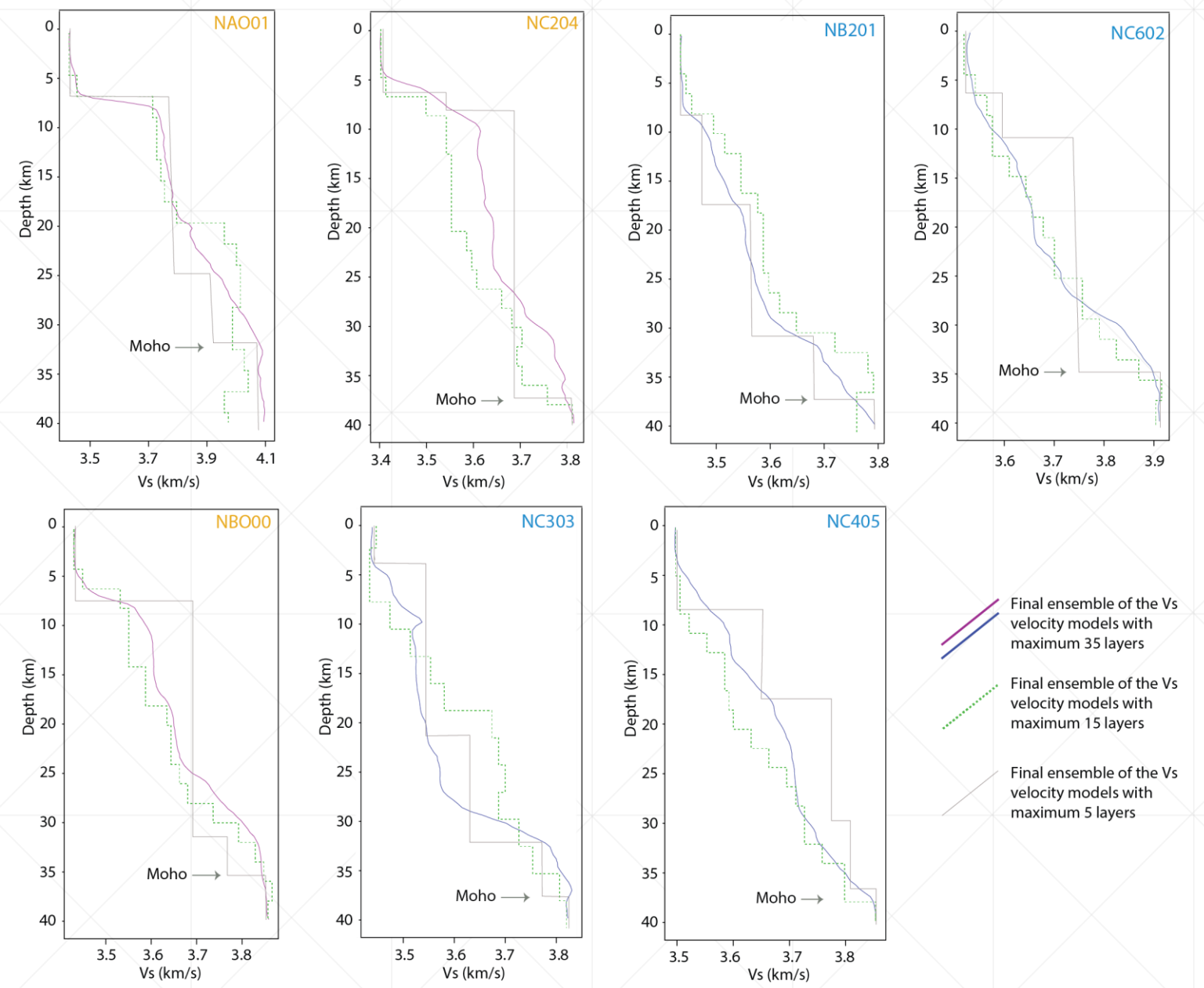
Figure 5: Schematic representation of a one-dimensional transdimensional model applied to receiver function inversion. m_i represents the velocity, which is the model unknown, but additionally the number of layers and their thicknesses are also a variable.

Velocity models

The velocity models were calculated using the receiver functions and the Rj-rf code available at the iEarth webpage (see references). The input parameters can be observed in **Table 3**:

Number of iterations	80000
Burn-in period	10000 iterations
Depth	0 – 40 km
Vs	3.30 – 4.50 km/s
Maximum number of partitions (layers)	35, 15, 5 for models 1, 2 and 3, respectively

Figure 6: Posterior ensemble showing the 1D S- wave velocity model for all stations. The seismic stations belonging to the western cluster are shown with an orange legend. Seismic stations corresponding to the eastern part, are shown with a light blue legend.



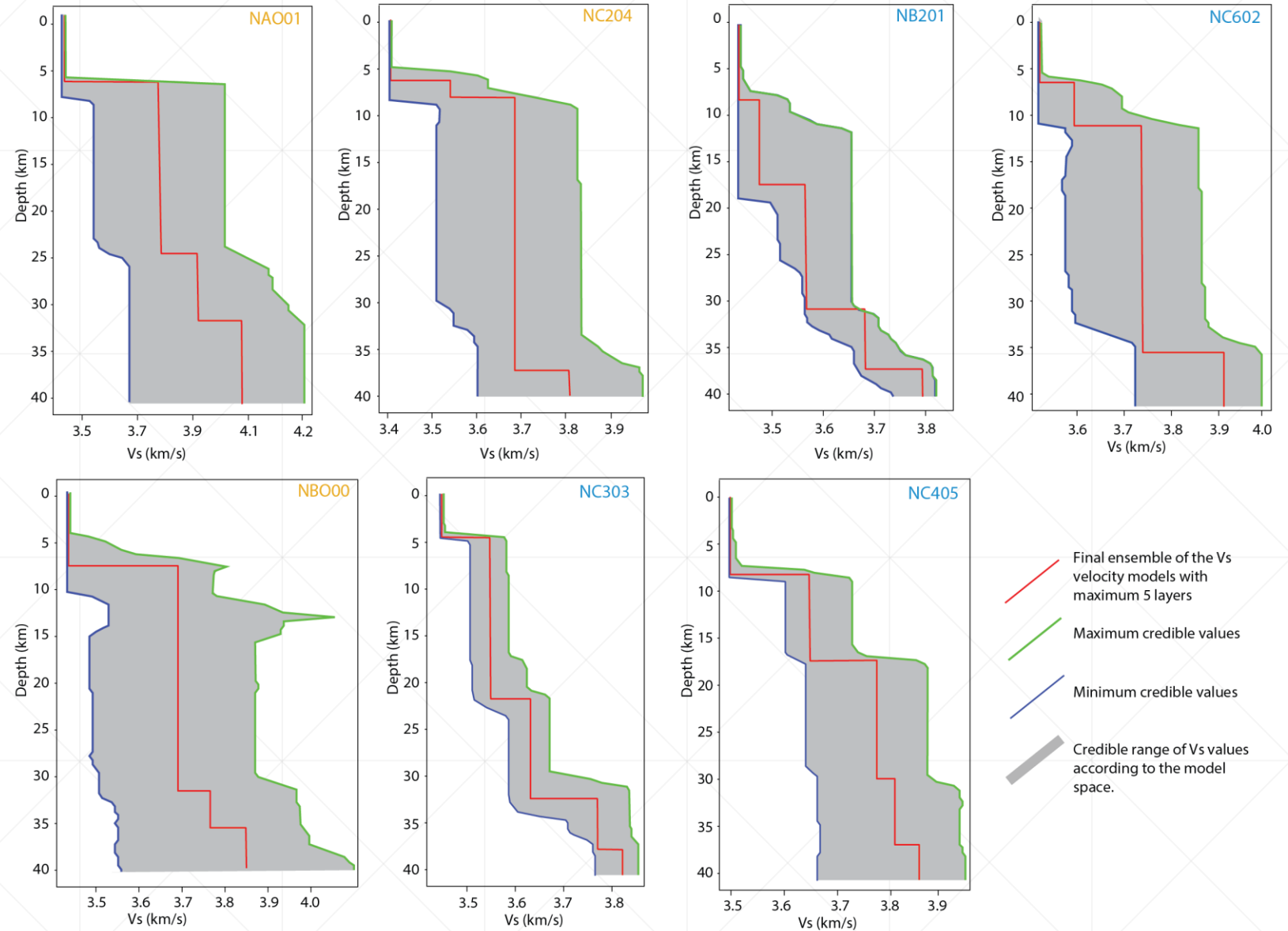
Final ensemble of the Vs velocity models with maximum 35 layers

Final ensemble of the Vs velocity models with maximum 15 layers

Final ensemble of the Vs velocity models with maximum 5 layers

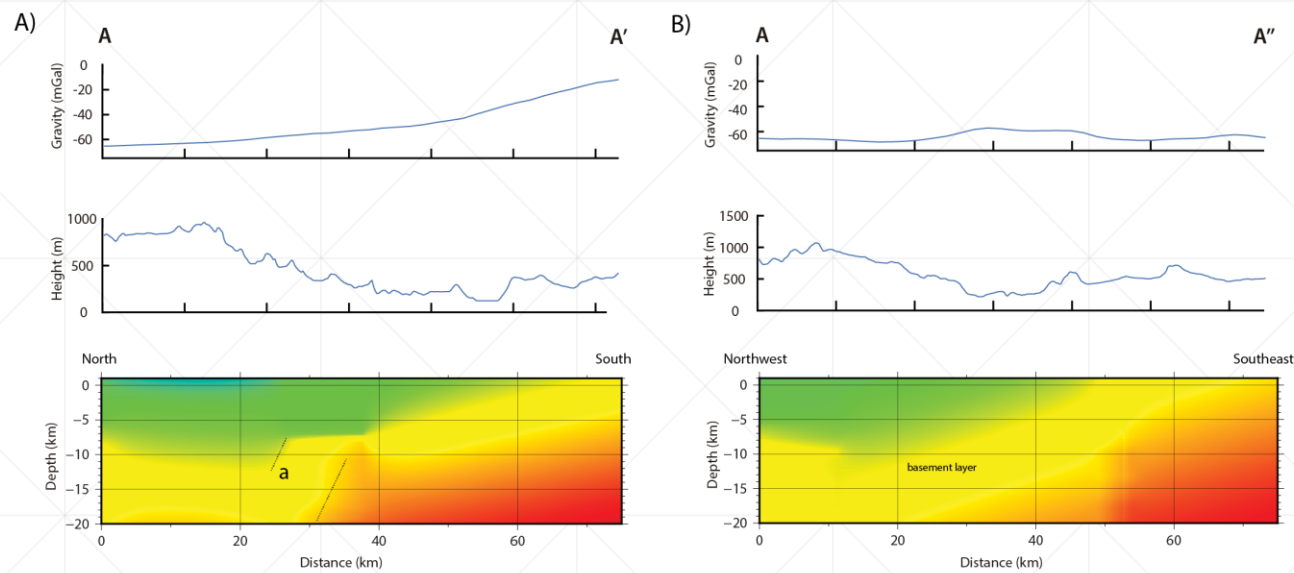
2D/3D density model

Figure 7: 1D S-wave velocity models delimiting the model space for all seismic stations. The gray shaded area shows the entire sampled model space. The colored lines represent the minimum credible values, the ensemble solution and the maximum credible values in blue, red and green, respectively.



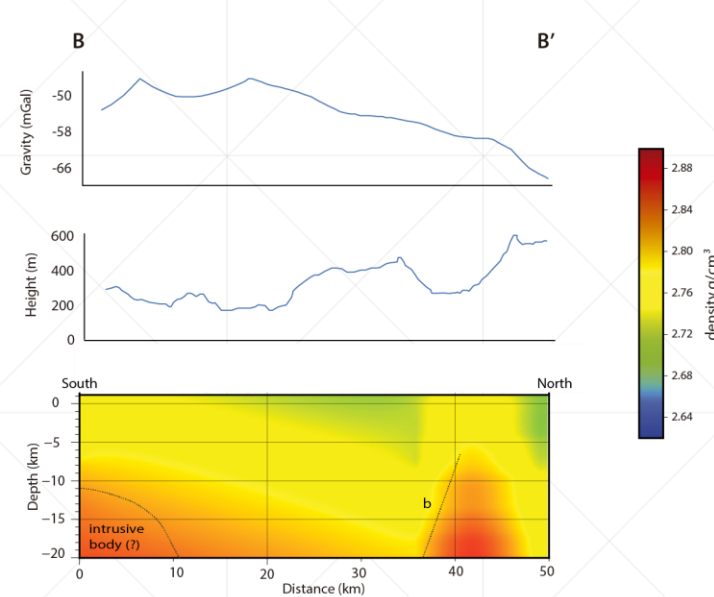
2D/3D density model

Figure 8: A, B & C correspond to the density models for the AA', AA'' and BB' cross sections. Additionally, topography and observed gravity are shown. Inferred thrust faults are marked with dotted lines. All profiles are using the same color palette.



Applying the Nafe-Drake curve, we obtained a velocity model from the Vp values.

It is possible to infer most likely NW dipping ENE-WSW striking major Normal faults in the Precambrian basement, which marks the tectonic boundary of the basin

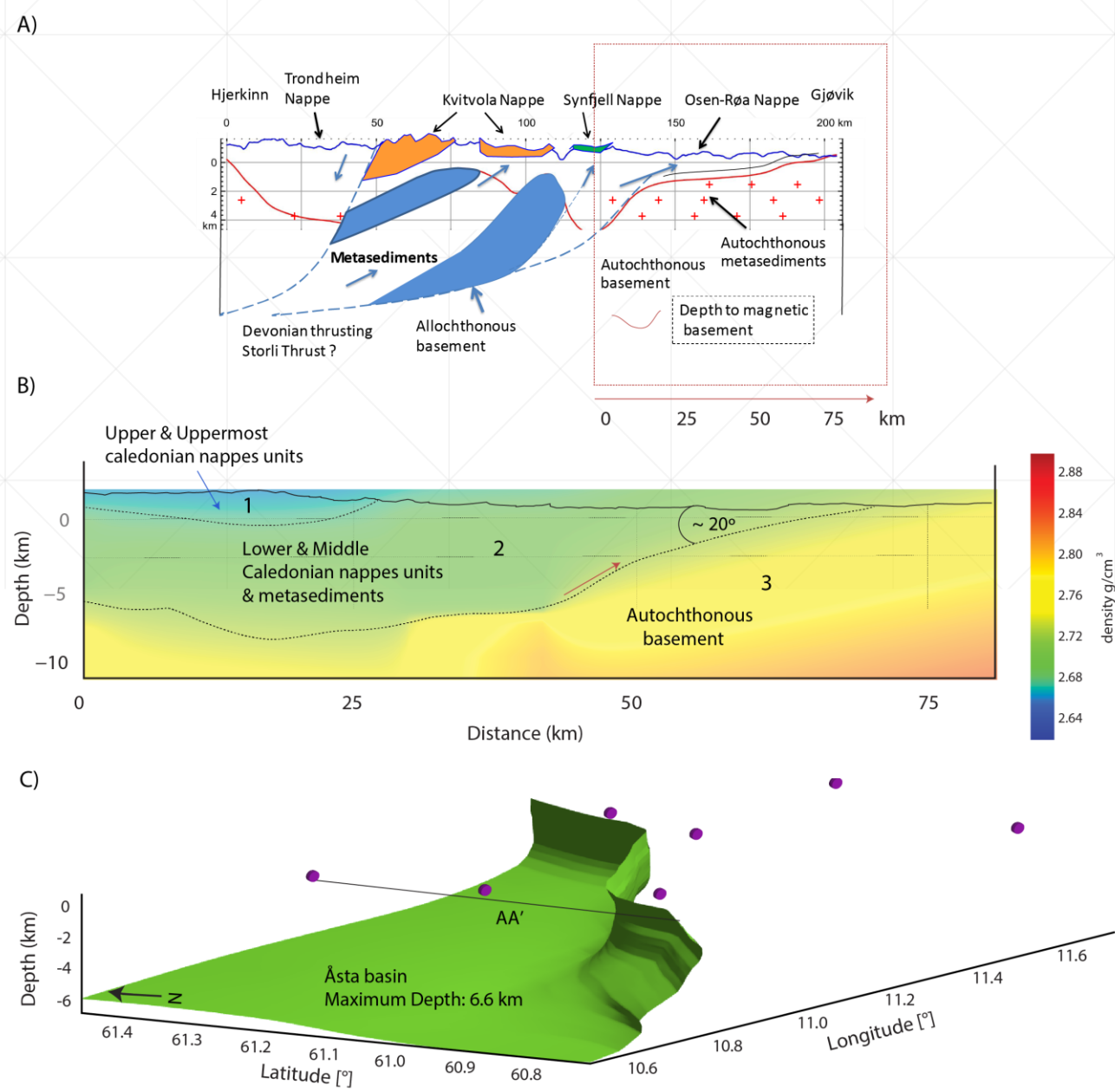


2D/3D density model

Figure 9: A. Geological cross section presented by Bjørlykke & Olesen (2018). Red dotted box is showing the subsection where the profile is compared with the AA' density model.

B. Density model for the AA' cross section, including the interpretation according to A).

C. 3D model showing the outline shape of the Åsta Basin. Purple dots correspond to the seismic network and position of the AA' profile is shown as a continuous black line.



Main references and funding source

This project was funded by the Chilean state through the Postdoctoral fellowship 'Postdoctorado en el extranjero Becas Chile 2019' project number 74200005 'Seismic Imaging using Norwegian Earthquakes'.

Additionally, this research was possible thanks to the support of the Geological Survey of Norway (NGU). The authors are also grateful for the IRIS Data Center freely providing the data applied for this research study.

Ammon, C. 1997. Personal webpage receiver function subsection
<http://eqseis.geosc.psu.edu/cammon/HTML/RftnDocs/rftno1.html>

Bjørlykke, A. & Olesen, O. 2018: Caledonian deformation of the Precambrian basement in southeastern Norway. *Norwegian Journal of Geology* 98, 1–16.

Bodin, T., Sambridge, M., Tkalčić, H., Arroucau, P., Gallagher, K. & Rawlinson, N. 2012: Transdimensional inversion of receiver functions and surface wave dispersion. *J. Geophys. Res.*, **117**, B02301. [doi:10.1029/2011JB008560](https://doi.org/10.1029/2011JB008560).

Hermann, R. 2013: Computer Programs in Seismology: An evolving tool for instruction and research. *Seismological Research Letters* 84. 1081–1088.

IEarth free software Rj-rf. <http://www.earth.org.au/codes/rj-RF/>.

Ligorria, J.P., Ammon, C.J. 1999: Iterative deconvolution and receiver-function estimation. *Bulletin of Seismological Society of America* 89 (5). 1395–1400.

Pavez, C., Brönnner, M., Bjørlykke, A., Olesen, O. 2020: Moho topography and velocity /density model for the Hedmarken area, Eastern Norway. NGU report 2020.013. 43 pp.

Sambridge, M., Bodin, T., Gallagher, K., Tkalčić, H. 2013: Trans-dimensional inference in the geosciences, *Phil. Trans. R. Soc. A*, 371, 20110547. [doi:10.1098/rsta.2011.0547](https://doi.org/10.1098/rsta.2011.0547).

Stratford, W., Thybo, H., Faleide, J.I., Olesen, O., Tryggvason, S. 2009: New Moho map for onshore southern Norway. *Geophysical Journal International* 178, 1755–1765.

Zhu, L. & H. Kanamori. 2000: Moho depth variation in southern California from teleseismic receiver functions. *Journal of Geophysical Research*, **105**, 2969–2980.